



Compatibility studies with pharmaceutical excipients for aripiprazole–heptakis (2,6-di-O-methyl)- β -cyclodextrin supramolecular adduct

Ionuț-Mihai Tănase¹ · Laura Sbârcea² · Adriana Ledeti³ · Paul Barvinschi⁴ · Denisa Cîrcioban³ · Gabriela Vlase⁵ · Renata-Maria Văruț⁶ · Ionuț Ledeti^{1,7}

Received: 9 January 2020 / Accepted: 3 June 2020 / Published online: 15 June 2020
© Akadémiai Kiadó, Budapest, Hungary 2020

Abstract

Aripiprazole (ARP) is one of the newest antipsychotic drugs, exhibiting very low aqueous solubility and high lipophilicity. Considering the necessity of improvement of ARP physicochemical properties and its biopharmaceutical profile, cyclodextrin complexation of the drug substance was performed. As selected cyclodextrin, a functionalized β -cyclodextrin was used, namely heptakis(2,6-di-O-methyl)- β -cyclodextrin (DIMEB), and the supramolecular adduct ARP/DIMEB was prepared by kneading technique and characterized using thermoanalytical tools (TG—thermogravimetry/DTG—derivative thermogravimetry/HF—heat flow), powder X-ray diffractometry patterns (PXRD), universal-attenuated total reflectance Fourier transform infrared (UATR-FTIR) and UV (ultraviolet) spectroscopy and, as well, saturation solubility studies. Job's method was used for the stoichiometry of APR/DIMEB inclusion complex determination, which was found to be 1:2. Molecular modeling studies were complementary realized as to get a view over the way that ARP is hosted inside the cyclodextrin. The compatibility between the inclusion complex and some common pharmaceutical excipients, namely starch, magnesium stearate, lactose monohydrate, microcrystalline cellulose and methylcellulose, has been evaluated by means of thermal methods of analysis (TG/DTG/HF), UATR-FTIR spectroscopy and PXRD pattern. The preformulation data regarding the compatibility of ARP/DIMEB complex with selected excipients suggested that under ambient conditions, chemical interactions are observed solely between ARP/DIMEB inclusion complex and magnesium stearate, as indicated by the UATR-FTIR spectroscopy. The incompatibility in the system ARP/DIMEB + MgS is also confirmed by the PXRD study, this second investigational technique revealing also the advanced amorphization of components during mixing of complex with starch, microcrystalline cellulose and methylcellulose, but without indicating interactions. Later on, under thermal stress, thermally induced interactions occur between the components in the systems containing magnesium stearate and methylcellulose, while starch, microcrystalline cellulose and lactose can be safely used as excipients in developing solid formulations containing ARP/DIMEB inclusion complex as active pharmaceutical ingredient.

Keywords Aripiprazole · Cyclodextrin · Inclusion complex · Thermal analysis · Excipient · Compatibility study

✉ Laura Sbârcea
sbarcea.laura@umft.ro

¹ Faculty of Industrial Chemistry and Environmental Engineering, Politehnica University of Timișoara, Vasile Parvan Street 6, 300223 Timișoara, Romania

² Department of Drug Analysis, Faculty of Pharmacy, “Victor Babeș” University of Medicine and Pharmacy, Eftimie Murgu Square 2, 300041 Timișoara, Romania

³ Department of Analytical Chemistry, Faculty of Pharmacy, “Victor Babeș” University of Medicine and Pharmacy, Eftimie Murgu Square 2, 300041 Timișoara, Romania

⁴ Faculty of Physics, West University of Timișoara, 4 Vasile Pârvan Blvd, 300223 Timișoara, Romania

⁵ Research Center for Thermal Analysis in Environmental Problems, Faculty of Chemistry-Biology-Geography, West University of Timișoara, 16 Pestalozzi Street, Timișoara, Romania

⁶ Department of Physical Chemistry, Faculty of Pharmacy, University of Medicine and Pharmacy Craiova, 2-4 Petru Rares Str, 200349 Craiova, Romania

⁷ Department of Physical Chemistry, Faculty of Pharmacy, “Victor Babeș” University of Medicine and Pharmacy, Eftimie Murgu Square 2, 300041 Timișoara, Romania

Introduction

Current therapeutic strategies for patients suffering of different psychotic disorders include the use of a novel functionalized quinolone derivative, namely 7-[4-[4-(2,3-dichlorophenyl)piperazin-1-yl]butoxy]-3,4-dihydro-1*H*-quinolin-2-one (structure presented in Fig. 1), known under common name of aripiprazole (ARP) [1].

ARP is mainly used in the treatment of manic episodes in both adult and pediatric subject, as monotherapy, and as well in the treatment of mania, bipolar disorders and schizophrenia [2–4].

The biopharmaceutical profile of ARP shows some inconveniences, due to its low aqueous solubility, making it a BCS (biopharmaceutics classification system) II class molecule. Its high lipophilicity requires the improvement of water solubility before developing pharmaceutical formulations [5]. Polymorphs and solvatomorphs of ARP are well known, and their physicochemical profile, including stability, dissolution behavior and solubility, is reported in the literature [6–8], along with crystalline transitions and their instrumental analysis [9–11].

Up to the date, several papers are published aiming toward improving ARPs physicochemical profile, including preparation of orodispersible films containing ball-milled ARP-poloxamer (R) 407 solid dispersions [12], self-microemulsifying drug delivery systems [13], pH-modulated solid dispersions using hot-melt extrusion technique [14], cocrystals with dihydroxy- and trihydroxybenzene cofomers [15], coprecipitation and nanomilling along with several excipients [16], salt formation [17], organic–inorganic nanohybrid systems containing montmorillonite [18], but as well formation of supramolecular adducts represented by inclusion complexes with native and/or functionalized cyclodextrins [19–21].

The importance of cyclodextrins in developing guest–host type supramolecular systems in pharmaceutical field is nowadays unquestionable, since numerous recent papers are devoted to these studies [22–32]. In our previous paper, we have presented the preparation and instrumental characterization for two inclusion complexes of ARP with two

functionalized β -cyclodextrins, namely random methyl- β -cyclodextrin (RAMEB) and heptakis(2,3,6-tri-O-methyl)- β -cyclodextrin (TRIMEB), both in solution and in solid state [21]. Our investigations followed other studies reported earlier in the literature, where the host molecule for ARP was beta-cyclodextrin (BCD) and hydroxypropyl-beta-cyclodextrin (HPBCD) [20], or solely HPBCD [19]. Also, ARP is formulated and commercialized on pharmaceutical market as injectable solution along with a functionalized cyclodextrin, namely sulfobutylether- β -CD [33].

Pharmaceutical dosage forms are the result of the active pharmaceutical ingredients (API) combination with excipients, these being various inactive pharmacological substances that are added in the final formulation for several reasons, such of improving stability, solubility and bioavailability of API, or making it more easily to be administered to patient; also, the adequate selection of excipient leads to formulations where biopharmaceutical properties can be modulated, and also increasing the shelf-time of it, in benefit to patients [34–38]. Preformulation studies are necessary, even if excipients are considered inert molecules, since during formulation stage and/or under storage of final formulation, interactions may occur even in solid state, leading to diminution of concentration of API, which is crucial, especially for drugs with narrow therapeutics index, which are incorporated in tablets in orders of micrograms [39, 40].

Since there no data were found in the literature regarding the compatibility between ARP/CDs inclusion complexes and pharmaceutical excipients, in this study we set our goal in studying the complexation of ARP with a methylated β -CDs, namely heptakis(2,6-di-O-methyl)- β -cyclodextrin (DIMEB) and later to evaluate the thermally induced interactions between the prepared complex and several excipients. In accordance with this, the selected list of excipients was represented by starch (STA), magnesium stearate (MgS), lactose monohydrate (LA), microcrystalline cellulose (CE) and methylcellulose (MCE), while the physicochemical characterization of samples included ultraviolet (UV) spectroscopy, thermoanalytical tools (TG/DTG/HF data), powder X-ray diffractometry (PXRD) and universal-attenuated total reflectance Fourier transform IR spectroscopy (UATR-FTIR).

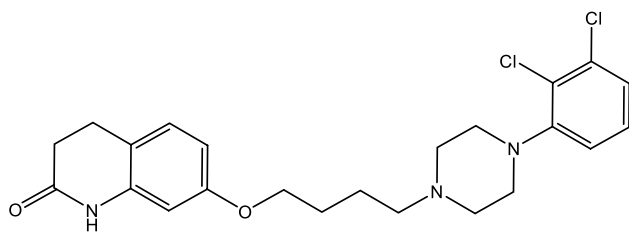


Fig. 1 Structural formula of aripiprazole (ARP)

Experimental

Materials

Aripiprazole (as Pharmaceutical Secondary Standard) was purchased from Sigma-Aldrich, and it was used as supplied by the producer. Heptakis(2,6-di-O-methyl)- β -cyclodextrin was a commercial product acquired from Cyclolab R&L Ltd (Budapest, Hungary). The pharmaceutical grade

excipients, namely starch, microcrystalline cellulose, magnesium stearate, lactose monohydrate and methylcellulose, were obtained from Sigma-Aldrich. All other used reagents, including solvents and salts, were of analytical purity.

Preparation of the ARP/DIMEB solid inclusion complex and physical mixtures

The ARP/DIMEB inclusion complex was obtained employing the kneading technique in 1:1 molar ratio. For the preparation of inclusion complex, a mass of 0.0760 g ARP and that of 0.2244 g DIMEB were accurately weighed. The mixture was triturated in an agate mortar in the presence of 0.30 g ethanol/HCl 0.1 M solution (1:1, m/m) until a homogeneous paste was obtained, for 45 min and under adding of few drops of solvent so that a suitable consistency is maintained. Later on, the product was dried under ambient conditions and then in an oven, at 40 °C for 24 h. The dried kneaded product was pulverized with the pestle and sieved through a 75- μ m size sieve.

For comparison, a physical mixture containing ARP and DIMEB in the same molar ratio as the inclusion complexes was prepared, by mixing in the agate mortar with pestle for 10 min, using a solvent-free technique.

The mixtures of ARP/DIMEB inclusion complex and each selected excipient were prepared by physically mixing in an agate mortar with pestle for approximately 5 min, in the ratio of 1:1 (m/m). This mass ratio was chosen in order to maximize the observation of possibly occurring interactions between components. The samples were then transferred in sealed vials and kept under ambient condition until the analysis was carried out, in the absence of light.

Study of formation of inclusion complex in solution

For all UV spectroscopy studies, a double-beam spectrophotometer SPECTRONIC UNICAM UV 300 UV–visible was used. All the measurements were realized in 1.0 cm matched quartz cells.

Analysis of stoichiometry and estimation of binding constant of inclusion complex

The stoichiometric ratio for interaction between ARP and DIMEB in formation of inclusion complex in solution was obtained according to the Job's method, employing a protocol elsewhere described [31]. Equimolar 9.00×10^{-5} M solution of ARP and DIMEB was prepared in 0.1 M acetate buffer at pH 4.0 and mixed to a standard volume, so that the ARP molar ratio varied from 0.1 to 0.9. Similar, a dilution set of ARP stock solution was prepared in the same solvent. After mixing, absorbances for all solutions were measured at the wavelength of 249 nm. The plot of the difference

between ARP absorbances, ΔA ($\Delta A = A - A_0$) in the presence (A) and in the absence (A_0) of DIMEB vs. ARP molar fraction R ($R = [\text{ARP}] / \{[\text{ARP}] + [\text{CD}]\}$) was built, according to our previous paper [21].

For the estimation of the apparent stability constants of the ARP/DIMEB supramolecular system, the method proposed by Benesi–Hildebrand was employed. The protocol was established earlier [21], so the ARP concentration was kept constant at 6.48×10^{-5} M in 0.1 M acetate buffer at pH 4.0, while the DIMEB concentration increased from zero to 5.184×10^{-3} M, in the same solvent. The UV spectra were collected in the spectral range 235–310 nm, using 1.0 cm matched quartz cells. All the experiments were carried out in triplicate, and the results were practical identical.

The association constant of the inclusion complex can be obtained from the Benesi–Hildebrand equations [21, 31, 41–43] for 1:2 guest–host inclusion complexes:

$$\frac{1}{\Delta A} = \frac{1}{\Delta \epsilon \cdot [\text{ARP}] \cdot K \cdot [\text{DIMEB}]^2} + \frac{1}{\Delta \epsilon \cdot [\text{ARP}]} \quad (1)$$

In the above equations, $\Delta \epsilon$ represents the variation of molar attenuation coefficient, ΔA is the variation of absorbance and K represents the stability constant.

Characterization of inclusion complex and physical mixtures in solid state

Thermal analysis

The pure ARP, DIMEB, excipients, the ARP/DIMEB physical mixture and kneaded product and the physical mixtures of ARP/DIMEB kneaded product with selected excipients were analyzed using a thermobalance produced by Perkin-Elmer DIAMOND TG/DTA under air atmosphere (flow rate of 0.1 L min^{-1}) under non-isothermal regime at a heating rate of 10 °C min^{-1} . For studying the thermal behavior of ARP, CD, kneaded product and all physical mixtures, samples with masses around 3–4 mg were weighted in aluminum crucibles and subjected to thermal stress in the 40–500 °C temperature domain. Simultaneous TG–thermogravimetry/DTG–derivative thermogravimetry/HF–heat flow data were collected. HF data (in mW) were obtained from DTA (differential thermal analysis) data (in μ V), by conversion.

Powder X-ray diffractometry (PXRD)

The PXRD analysis was carried using a diffractometer produced by Bruker, model D8 Advance powder X-ray. The X-ray diffraction patterns were collected with $\text{CuK}\alpha$ radiation and a Ni filter over the interval of 5°–45° angular domain (2θ). The instrument was operated at 40 kV and 35 mA.

Universal-attenuated total reflectance Fourier transform infrared spectroscopy

The FTIR spectra were recorded using a Perkin-Elmer SPECTRUM 100 device. The data were collected directly on solid samples using an UATR device in the spectral domain 4000–600 cm^{-1} . Spectra were drawn up after 16 co-added scans, with a spectral resolution of 4 cm^{-1} .

Molecular modeling

Gaussian program suite at DFT/B3LYP/6-311G optimization was used in order to generate the three-dimensional (3D) coordinates of ARP. To visualize the interaction between ARP and DIMEB, the molecular docking analysis was performed using AutoDock 4.2.6 software along with the AutoDockTools. The heptakis (2,6-di-O-methyl)- β -cyclodextrin structure was generated from the curated coordinates of ligand 2QKH (X-ray diffraction, resolution 1.9 Å) downloaded from the Protein Data Bank database [44]. Methyl groups were manually added on free hydroxyl groups from 2 and 6 positions (GaussView 5, Semichem Inc.), structure being optimized in the same manner with ARP (DFT/B3LYP/6-311G).

Two consecutive docking cycles were carried out since a single molecule of ARP was expected to accommodate with 2 molecules of DIMEB and the best result from each cycle was chosen. DIMEB dimers were obtained from two identical DIMEB molecules aligned on the cavity axes, having the outer sides pointing one to another. Two molecules of DIMEB were used in the first docking, one as a receptor and the other as a ligand in order to get the best configuration of the dimer complex and to compute the total energy of affinity (kcal/mol). In the second docking, ARP was used as ligand and DIMEB dimer as receptor.

The obtaining of DIMEB dimers molecule and the docking between ARP and dimers involves adding all the polar hydrogen atoms, computing the Gasteiger charge; grid box was generated using Autogrid 4 with $60 \times 60 \times 60$ Å in x , y and z axis with 0.375 Å spacing from receptor center. All the calculations were carried out in vacuum.

The Lamarckian genetic algorithm with a population size of 150 and 50 runs was selected for the docking study. All other parameters were used with default values. Molecular modeling figures were obtained using PyMOL software [45].

Evaluation of solubility behavior of kneaded product

For the investigation of solubility change due to the inclusion complex formation, the saturation shake-flask method was used. For this purpose, an excess amount of ARP and ARP/DIMEB kneaded product was added in 5.0 mL of acetate

buffer 0.1 M at pH 4.0, so that saturation was achieved. All the protocols for sample preparation and estimation of ARP concentrations were previously reported [21].

Results and discussion

Study of formation of inclusion complex in solution

Analysis of stoichiometry and estimation of binding constant of inclusion complex

All the data were processed according to Job's method [46]. The stoichiometry of the inclusion complex can be obtained when a measurable property that correlates linearly with the complex concentration (such as absorbance A) is plotted versus guest molar fraction. The complexation stoichiometry is provided by the value of the molar ratio R , which indicates the maximum concentration of the complex [31, 47, 48]. The value of R at the maximum deviation (ΔA) is reached when ARP molar fraction is 0.33 (Fig. 2), which suggests a stoichiometry of 1:2 of ARI in the complex.

The association constant of the ARP/DIMEB inclusion complex was estimated based on Benesi–Hildebrand model [21, 31, 42]. Changes in the UV absorption intensity of the ARP at 249 nm have been evaluated as a function of DIMEB concentration. An increase in ARP absorption intensity as a result of increasing DIMEB concentrations has been observed (Fig. 3a), along with a bathochromic shift in the absorption maxima of ARP, proving that the inclusion complex was formed.

In order to confirm the stoichiometry for ARP/DIMEB complex, a double-reciprocal plot was built, namely ΔA^{-1} versus $[DIMEB]^{-2}$, as shown in Fig. 3b. Good linear correlation was obtained in the plot ($R^2 = 0.9878$), confirming

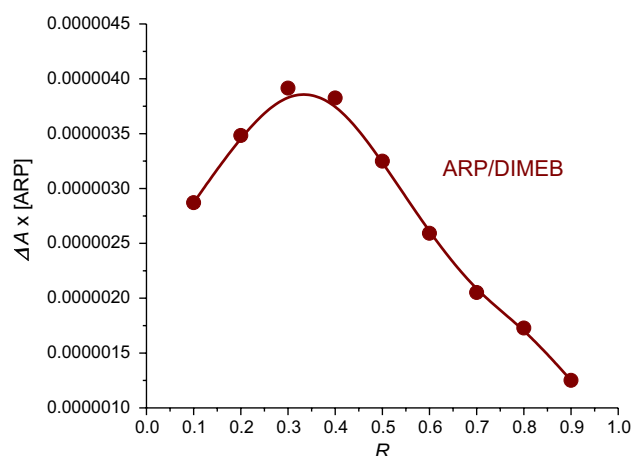


Fig. 2 Job's plot corresponding to the ARP/DIMEB inclusion complex

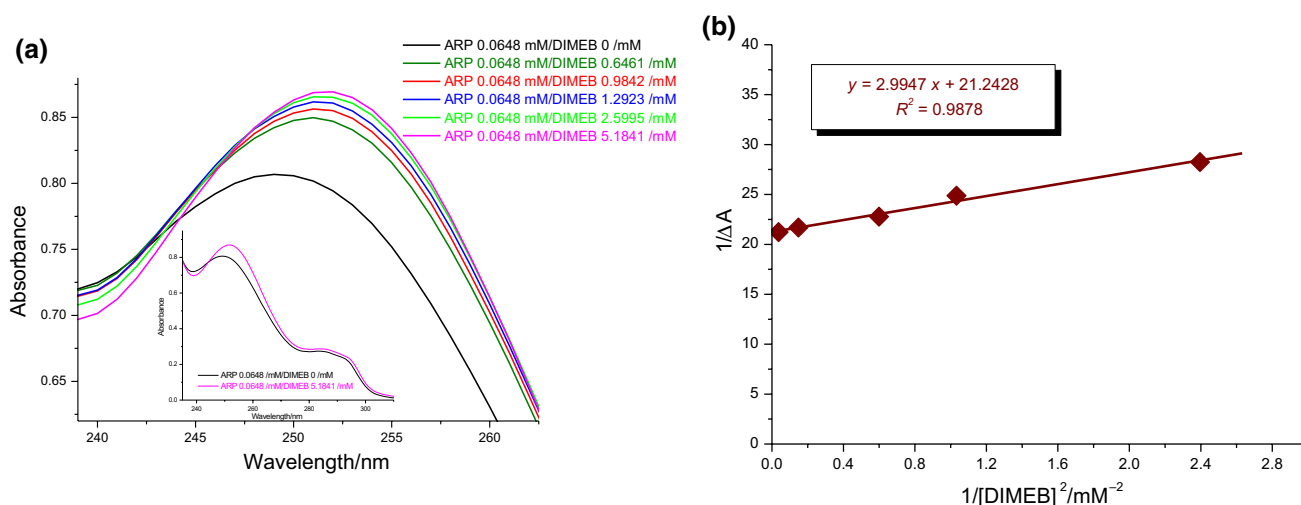


Fig. 3 UV spectra of ARP and ARP/DIMEB adduct in the presence of increasing concentration of DIMEB, in 240–262 nm spectral range—main image; UV spectra of ARP and ARP/DIMEB at

maximum DIMEB concentration, in 235–310 nm spectral domain—inserted image **a**; Benesi–Hildebrand linear plots for ΔA^{-1} against $[DIMEB]^{-2}$ **b**

the formation of the inclusion complex with 1:2 stoichiometry. The stability constant value was evaluated using Benesi–Hildebrand Eq. (1) as a ratio of the intercept to slope of the straight line in the Benesi–Hildebrand double reciprocal plot, and the calculated value is $7.09 \times 10^6 \text{ M}^{-2}$.

Characterization of solid-state inclusion complex

Thermal analysis

Among the techniques used for the study of the host–guest interaction during the inclusion complex formation, the thermal analysis leads to valuable results. The peak of phase transitions, such as melting of the guest molecules entrapped in the CDs cavity, is generally shifted to a different temperature in comparison to pure API or even disappears [49]. The thermal curves (TG/DTG/HF) of ARP, DIMEB and ARP/DIMEB prepared as simple physical mixture (PM) and kneaded product (KP) are shown in Fig. 4a–d.

Interpretation of thermoanalytical data recorded for ARP is elsewhere discussed in detail [21]. Since the thermoanalytical profile of the pure API was recorded in identical conditions as in our previous paper, the obtained results are practical identical [21], suggesting that the first mass loss begins at 148 °C, reaching a DTG_{max} at 149 °C, probably associated with release of water traces ($\Delta m = 0.4\%$). The main decomposition process of ARP starts at 220 °C, reaching the DTG_{max} around 302 °C and takes place in one step. Since no thermal oxidations occur up to 220 °C, it can be said that ARP has a good thermal stability after the insignificant mass loss that takes place around melting. HF curve reveals two endothermic events,

the first at 139 °C corresponding to the solid–liquid transition of polymorphic form III, followed by another one at 149 °C, corresponding to the solid–liquid transition of polymorphic form I. The peritectic melting of ARP was previously discussed [21]. The main exothermic process due to oxidative thermolysis of ARP is revealed by the HF curve, which shows a peak at 316 °C, being in excellent agreement with previously reported data [21].

The thermal curves of DIMEB reveal that the cyclodextrin is thermally stable up to 232 °C, when the decomposition process starts, reaching DTG_{peaks} at 343 and 353 °C, respectively. The exothermic effects from the HF curve ($T_{peak} = 252$ and 360 °C, respectively) are related to the thermooxidation processes of the cyclodextrin, DIMEB melting being probably overlapped with these events [50].

The thermoanalytical curves of ARP/DIMEB binary system present differences as compared with those of the parent compounds (Fig. 4). Thus, the endothermic melting peak of ARP form III has disappeared from the HF curves of ARP/DIMEB KP and has been shifted to lower temperature ($T_{peak} = 131.3$ °C) in the HF curve of ARP/DIMEB PM. Also, the endothermic melting event of ARP form I is no longer present neither in the HF curve of KP nor in the HF curve of PM (Fig. 4d). Furthermore, the DIMEB decomposition exothermic peak is shifted toward higher temperature in the HF diagrams of both KP ($T_{peak} = 302.3$ °C) and PM ($T_{peak} = 366.8$ °C). A greater thermal stability of ARP is revealed by the thermoanalytical curves of the binary systems, since the drug decomposition begins around 228 °C and 251 °C for KP and PM respectively, as the thermal curves show (Fig. 4c, d).

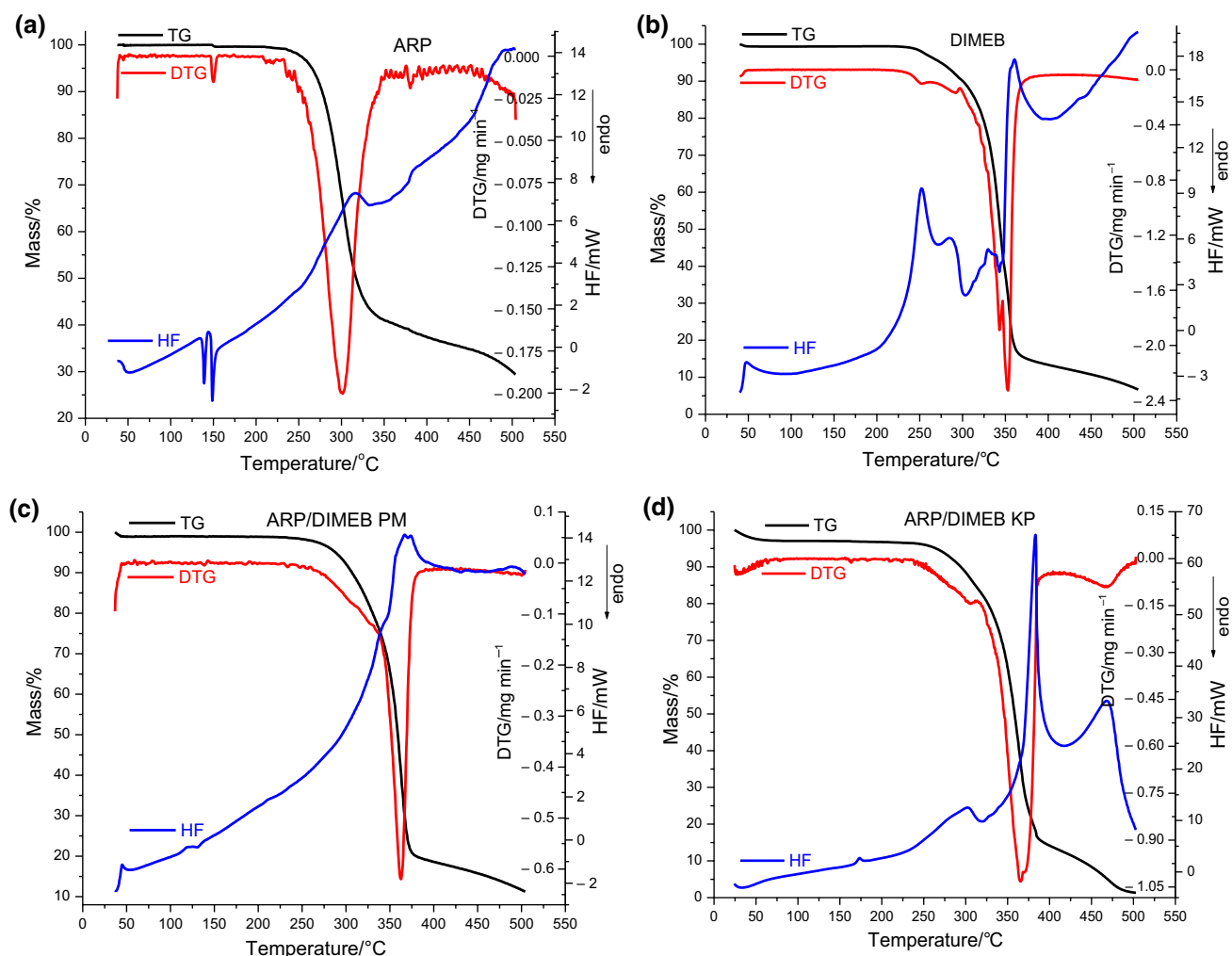


Fig. 4 Thermoanalytical curves TG, DTG and HF for: **a** ARP; **b** DIMEB; **c** ARP/DIMEB PM and **d** ARP/DIMEB KP in air atmosphere (0.1 L min^{-1}), 40–500 °C temperature range at a heating rate $\beta = 10 \text{ °C min}^{-1}$

The absence of the melting processes of ARP form III and form I from the thermal profile of the ARP/DIMEB kneaded product indicates ARP involvement in the complexation process. The results provided by thermal analysis demonstrate the existence of an interaction between ARP and DIMEB and confirm inclusion complex formation under kneading.

Powder X-ray diffractometry

The diffractometry profile of ARP, DIMEB and their PM and KP is shown in Fig. 5.

The ARP diffraction pattern indicates the presence of two peaks of higher intensity at 2 value of 20.38 and 22.04 and other several secondary peaks at 11.02; 14.36; 16.54

and 19.39 2, revealing its crystalline nature (Fig. 5), as reported earlier [21]. In the diffraction pattern of DIMEB, the appearance of sharp peaks at 8.54, 9.95, 10.29, 12.31, 16.89, 19.04 and 21.32 2 demonstrates that DIMEB has a crystalline structure. The examination of PXRD patterns of the binary compounds reveals major changes in relation to the pure substances. The ARP/DIMEB PM diffractogram shows a marked diminution of the characteristic diffraction peaks of ARP and DIMEB, respectively. In addition, the presence of two broad peaks and many undefined, diffused peaks with low intensities is noticed in both PM and KP diffraction patterns, reflecting the amorphous state of the samples (Fig. 5). The disappearance of the ARP

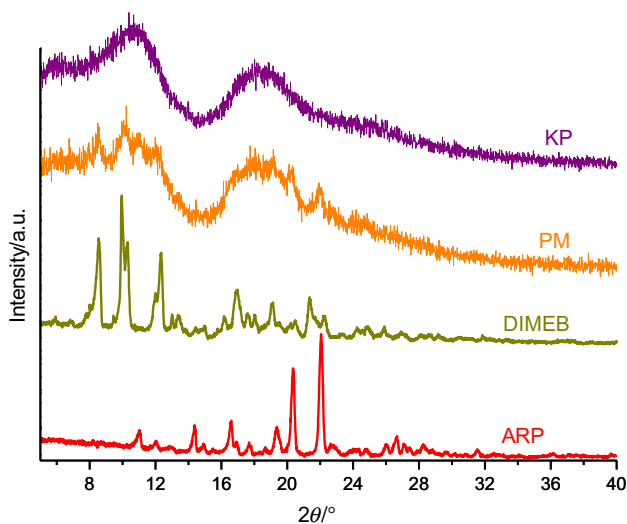


Fig. 5 PXRD patterns recorded for ARP, DIMEB, ARP/DIMEB PM and ARP/DIMEB KP

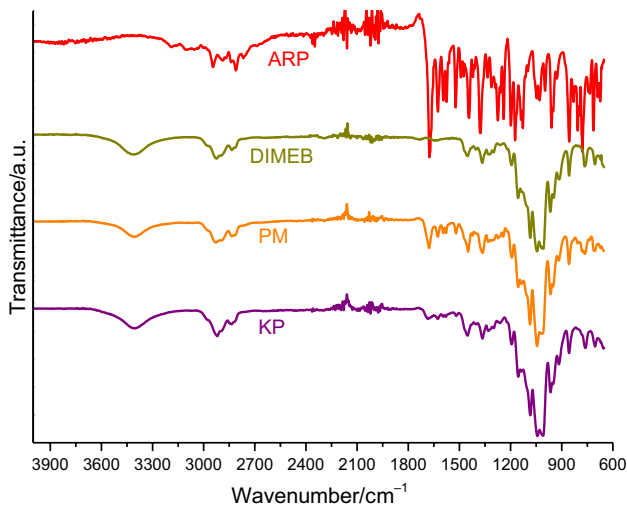


Fig. 6 UATR-FTIR spectra of ARP, DIMEB, ARP/DIMEB PM and ARP/DIMEB KP samples

characteristic peaks in the ARP/DIMEB KP diffractogram suggests the interaction of API with CD and demonstrates the formation of the inclusion complex in solid state, in good agreement with the results suggested by thermoanalytical techniques.

UATR-FTIR analysis

The UATR-FTIR spectra of ARP, DIMEB and binary mixtures represented by ARP/DIMEB PM and ARP/DIMEB KP are shown in Fig. 6.

The UATR-FTIR spectrum of ARP shows characteristic bands of polymorphic form III, as previously described in detail [21]. In order to identify the characteristic bands of ARP in binary mixtures with DIMEB, the wavenumbers of the main bands are presented here without association with functional groups from the structure of the antipsychotic drug (in cm^{-1}): 3192, 2945, 2812, 1676, 1627, 1594, 1576, 1522, 1444, 1375, 1259, 1047, 1030, 806 and 778, respectively.

DIMEB exhibits a broad absorption band in the 3500–3300 cm^{-1} spectral region assigned to O–H stretching vibration from the non-methylated hydroxyl moieties and a large region below 1500 cm^{-1} which displays distinct peaks, most probably characteristic to the cyclodextrin ring [50, 51].

The IR spectra of both ARP/DIMEB KP and PM reveal differences in comparison with those of the pure substances. Therefore, the absorption band at 1676 cm^{-1} assigned to the stretching vibration of ARP carbonyl group was shifted to 1678 cm^{-1} in the PM spectrum and to 1686 cm^{-1} in the KP spectral pattern and the intensity of band was diminished. Similarly, the peaks associated with the C–H bending vibration shifted from 1444 to 1375 cm^{-1} in the pure ARP to 1449 and 1364 cm^{-1} in the PM spectrum and to 1452 and 1363 cm^{-1} in the KP spectrum. The characteristic bands for the N–H bending vibration at 1627 cm^{-1} and for the aromatic ring (1594 and 1576 cm^{-1}) are still present in the PM, but their intensity was diminished, while they were disappeared from the KP spectrum. Also, the peak corresponding to N–H stretching vibration situated at 3192 cm^{-1} in pure ARP spectrum is no more present in the spectra of ARP/DIMEB PM and KP, most probably due to the formation of H-bonding between drug substance and CD. Therefore, it can be seen that the characteristic peaks of drug substance either have reduced their intensity along with shifting to different wavenumbers or have disappeared in the binary products, these changes indicating the interactions between ARP and DIMEB molecule.

Molecular modeling

AutoDock provides docking tools, being able to predict the binding interaction that takes place between small molecules

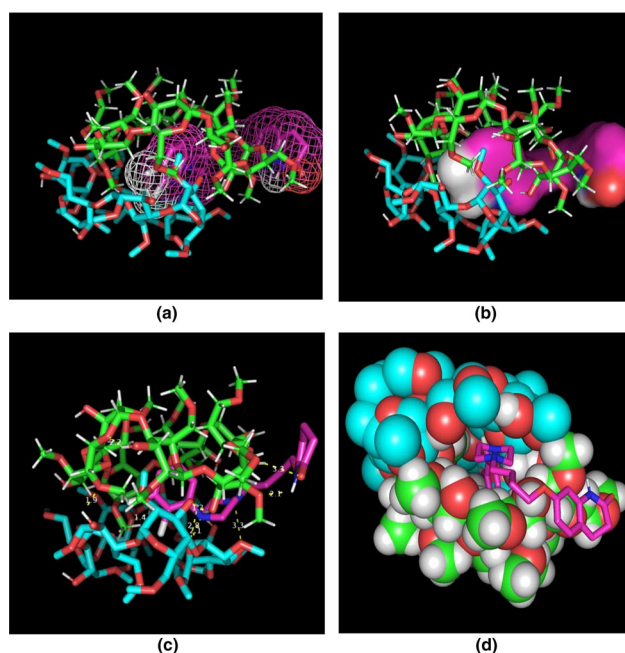


Fig. 7 Molecular geometry of the inclusion complex ARP/DIMEB in 1:2 molar ratio. Images **a**, **b** and **d** show the inclusion complex from the narrow rim of DIMEB's cavity. ARP guest molecules are shown in mesh/surface/sticks colored by element, while DIMEB is represented in green and blue. Image **c** shows polar contacts between ARP and DIMEB, ARP being colored in purple and DIMEBs, in blue and green

(ligand), to a known 3D-structured receptor. The theoretical basis of AutoDock was elsewhere presented [21, 52].

Molecular modeling was employed for a detailed characterization of the inclusion complex ARP/DIMEB (1:2), the calculated binding free energy value being $-6.02 \text{ kcal mol}^{-1}$. The theoretical structural geometry of ARP/DIMEB inclusion complex, as generated in PyMOL software, simulated in 1:2 molar ratio is shown in Fig. 7.

Three hydrogen bonds between ARP and DIMEB are formed as the 3D images of the ARP/DIMEB 1:2 interaction revealed. The hydrogen bonds are established between the heterocyclic nitrogen atom from the piperazine moiety (namely the N-butoxylated one) and the OH (position 3) of the dimer, with a length of 3.3 \AA , and between the nitrogen from N-aryl-substituted piperazine moiety and the oxanic oxygen of the dimer, with a length of 2.1 \AA . The third intermolecular interaction represented by a H-bonding occurs between the hydrogen belonging to NH group from the 2-piperidinone heterocyclic moiety and the hydroxyl (position 6) of dimer glucopyranose unit with a length of 2.1 \AA . The presence of Keesom-type dipole-dipole interaction between the carbonyl oxygen of

the 2-piperidinone heterocycle and the oxygen hydroxyl (position 6) of a glucopyranose unit is also to be noticed having a length of 2.3 \AA .

Solubility profile of kneaded product

The solubility of the drug substance in the ARP/DIMEB KP was evaluated by means of shake-flask technique [53–55]. The ARP concentration in the saturated solution was determined using UV spectrophotometric measurements and a calibration curve of ARP, at $25 \text{ }^\circ\text{C}$ [21]. The solubility of the included ARP was calculated to be $2237.822 \pm 0.011 \text{ } \mu\text{g mL}^{-1}$ as a mean value of five experimental measurements. In standard controlled experiments, clear solutions were obtained by dissolving 44.4 mg of ARP/DIMEB KP in 5.0 mL 0.1 M acetate buffer of $\text{pH} = 4.0$, at room temperature.

The saturation solubility studies demonstrate the efficiency of DIMEB in the solubility enhancement of this practically water-insoluble drug (ARP). A 37.87-fold increment in the solubility of ARP in 0.1 M acetate buffer of $\text{pH} = 4.0$ in the presence of DIMEB as compared to free ARP ($59.09 \text{ } \mu\text{g mL}^{-1}$) was noticed due to the solubilizing effect of this functionalized CD.

Compatibility studies of ARP/DIMEB inclusion complex with pharmaceutical excipients

TG/DTG/HF analysis

TG/DTG/HF curves recorded in dynamic air atmosphere at $\beta = 10 \text{ }^\circ\text{C min}^{-1}$ for ARP/DIMEB inclusion complex and the mixtures of inclusion complex with excipients are presented in Fig. 8a–d.

The thermoanalytical profile of the ARP/DIMEB inclusion complex (Fig. 4d) reveals its thermal decomposition in the following temperature ranges: $35\text{--}70 \text{ }^\circ\text{C}$ ($\Delta m = 2.7\%$, due to dehydration), $167\text{--}330 \text{ }^\circ\text{C}$ ($\Delta m = 19.3\%$, $\text{DTG}_{\text{peak}} = 305.6 \text{ }^\circ\text{C}$), $330\text{--}290 \text{ }^\circ\text{C}$ ($\Delta m = 62.5\%$, $\text{DTG}_{\text{peak}} = 365.5 \text{ }^\circ\text{C}$) and $390\text{--}500 \text{ }^\circ\text{C}$ ($\Delta m = 15.5\%$, $\text{DTG}_{\text{peak}} = 468.1 \text{ }^\circ\text{C}$). The HF profile of the inclusion complex reveals the presence of four exothermic events, the first one presenting low intensity and a maximum at $173.6 \text{ }^\circ\text{C}$, and the other three in the $250\text{--}500 \text{ }^\circ\text{C}$ temperature domain with maximum at $302.3 \text{ }^\circ\text{C}$, $383.3 \text{ }^\circ\text{C}$ and $469.4 \text{ }^\circ\text{C}$, respectively, that correspond to the decomposition of the complex.

In the situation of inclusion complex–excipients physical mixtures (Fig. 8), the evaluation of TG/DTG curves indicates that the mass loss processes are noticed in the same

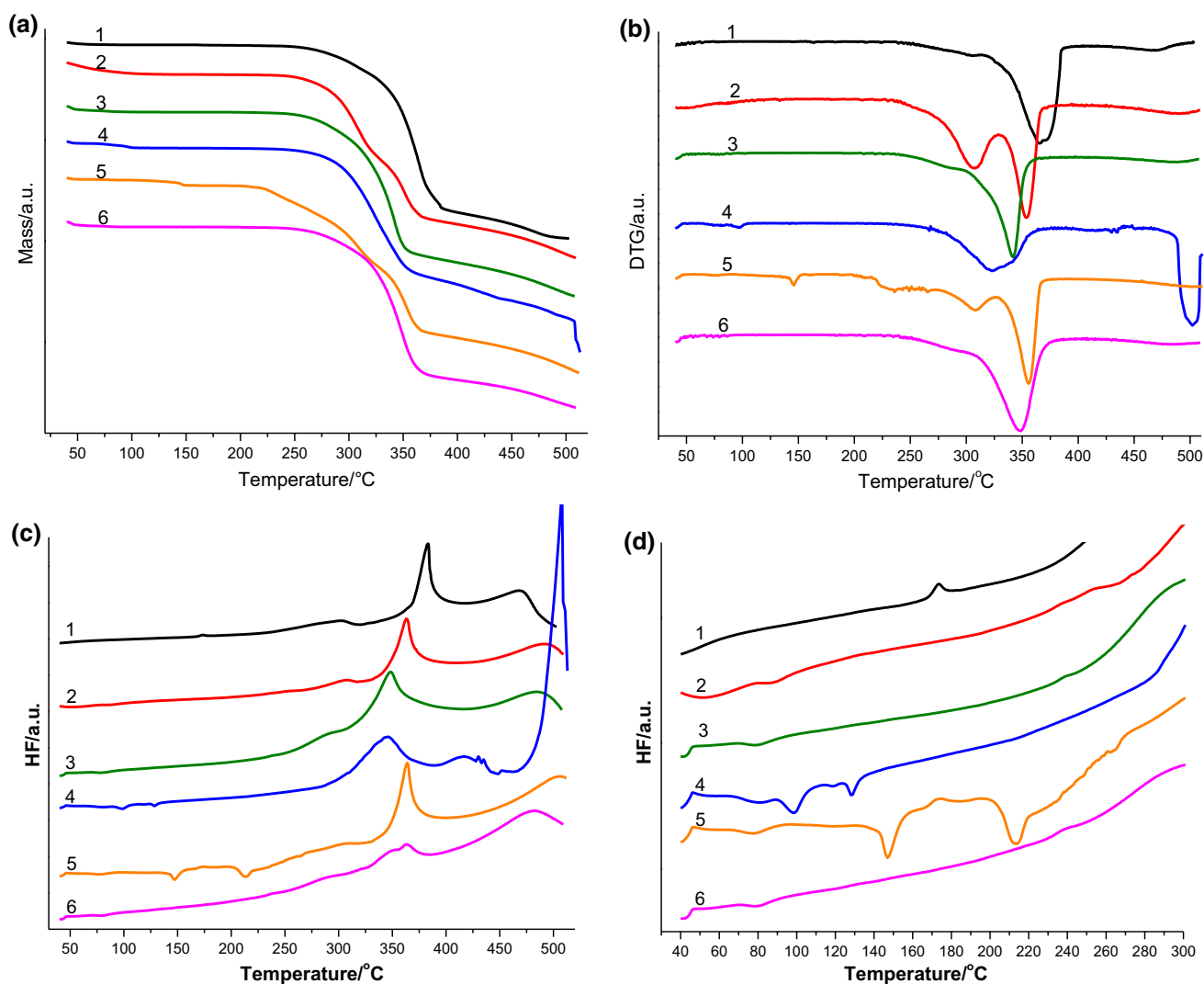


Fig. 8 TG **a**, DTG **b** and HF (**c** temperature range of 40–500 °C; **d** temperature range of 40–300 °C) curves drawn up in air, at $\beta=10$ °C min^{-1} for ARP/DIMEB inclusion complex (1) and inclusion com-

plex-excipients mixtures, as follows: (2) ARP/DIMEB+STA; (3) ARP/DIMEB+CE; (4) ARP/DIMEB+MgS; (5) ARP/DIMEB+LA and (6) ARP/DIMEB+MCE

temperature range as for the ARP/DIMEB pure complex, excepting the mixture ARP/DIMEB+LA. All the rest mixtures display a mass loss at temperatures lower than 70 °C due to the release of water, then being stable up to temperature values around 200 °C. With further increase of temperature, the main stage of mass loss due to thermal degradation process arises between 205 and 403 °C in the case of ARP/DIMEB+STA mixture (DTG_{peak} at 308 and 354 °C), in the temperature range of 215–389 °C for ARP/DIMEB+CE (DTG_{peak} at 342 °C), between 225 and 383 °C for mixture with MgS (DTG_{peak} at 346 °C) and between 210 and 394 °C (DTG_{peak} at 348 °C) in the case of ARP/DIMEB+MCE.

The TG/DTG profile of the mixture with LA expresses a mass loss event up to 170 °C associated with dehydration of excipient, followed by a narrow stability stage in the temperature range of 170–200 °C, and then, the mass loss continues with the main decomposition event between 200 and 400 °C (DTG_{peak} at 236, 308 and 356 °C, respectively).

Regarding the HF profile of all complex-excipients mixtures, the exothermic event of low intensity is missing from all curves (Fig. 8d), while the main exothermic event from HF curve of the complex, with maximum at 383.3 °C was preserved but shifted to a lower temperature in the HF curves of the physical mixture as follows: 363 °C in case of ARP/

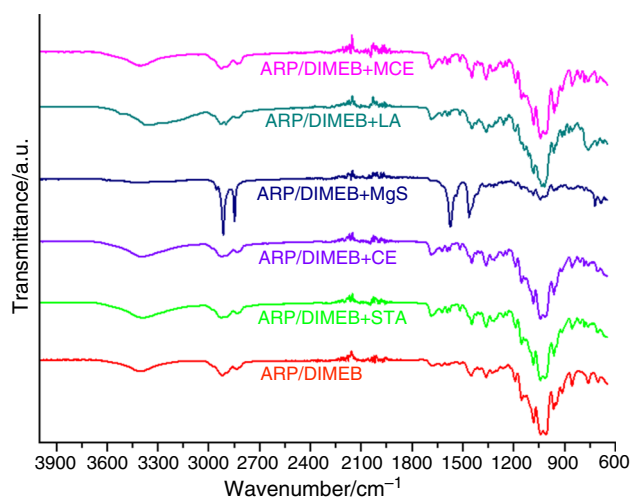


Fig. 9 UATR-FTIR spectra recorded for ARP/DIMEB inclusion complex and its binary mixtures with selected excipients

DIMEB + STA and ARP/DIMEB + MCE, 348 °C for the mixture with CE, 346 °C in the presence of MgS and 364 °C for the ARP/DIMEB + LA (Fig. 8c). These significant shifts to lower temperature may indicate a potential incompatibility between ARP/DIMEB inclusion complex and the excipients taken into study, at advanced thermal treatment. On the other hand, shifting of ARP/DIMEB exothermic event to lower temperature may be the result of mixing with the excipients which decrease the purity of every component in the mixture, as previously stated in the literature [56]. The identification of nature of thermally induced interaction between the complex and each excipient (namely a chemical interaction versus a physical depression of melting point due to the presence of “impurities,” represented here by the molecules of excipient) can be tentatively presented based on the analysis of HF profile for the main exothermic event occurring over 275 °C, as follows: for mixtures with STA, CE and LA, the thermoanalytical profile is similar as for pure complex (Fig. 8), while for MgS and MCE, the profile is considerable modified. Taking these observations into

account, it can be suspected that thermally induced interactions take place in the systems containing MgS and MCE, while the impurity effect of excipient is noticed in systems containing STA, CE and LA.

Following the data of the compatibility studies between ARP/DIMEB inclusion complex and selected excipients by using thermal analysis, we can conclude that possible interaction occurs between the components of the physical mixtures. Therefore, complementary techniques, such as FTIR and PXRD, were further used in order to get an objective view over the compatibility of the components of these systems under ambient conditions.

UATR-FTIR studies

UATR-FTIR technique is a valuable tool used for revealing the potential physicochemical interaction between an API and the selected excipients used. The chemical modifications which occur due to the interaction at the reactive functional groups of API and excipient cause the shifting toward different wavenumbers and the appearance or disappearance of characteristic bands for “reactive” moieties of API in multicomponent systems when compared with pure drug substance [57]. The UATR-FTIR spectra of ARP/DIMEB inclusion complex and its mixtures with tested excipients recorded in ambient temperature are presented in Fig. 9.

The FTIR spectrum of ARP/DIMEB inclusion complex presents a broad band between 3500 and 3300 cm^{-1} (peak at 3404 cm^{-1}) which is indicative of hydroxyl groups (O–H stretching vibration) and other several bands, which are noticed in Table 1 and are presented in “*Characterization of solid-state inclusion complex*” section. The carried out investigations based on spectra results depicted in Fig. 9 and data collected in Table 1 reveal that the majority of ARP/DIMEB characteristic bands arise in the binary mixture either at the same wavenumber as in the complex or are slightly shifted to different wavenumbers—suggesting lack of chemical interactions between the complex and the selected excipients, except for the mixture with MgS. In this

Table 1 UATR-FTIR bands of ARP/DIMEB inclusion complex and the mixtures with excipients

Sample	Analysis of UATR-FTIR spectral regions/ cm^{-1}		
	3600-2700	1700-1000	1000-650
ARP/DIMEB	3404; 2930; 2848	1686; 1452; 1363; 1194; 1155; 1084; 1043; 1010	966; 917; 857; 761; 704
ARP/DIMEB + STA	3394; 2928; 2835	1685; 1450; 1365; 1191; 1155; 1084; 1044; 1013	964; 919; 857; 763; 706
ARP/DIMEB + CE	3390; 2925; 2834	1686; 1450; 1365; 1191; 1156; 1085; 1044; 1018	964; 917; 857; 762; 704
ARP/DIMEB + MgS	2916; 2850	1686; 1464; 1366; 1190; 1086; 1045; 1018	963; 876; 722; 686
ARP/DIMEB + LA	3345; 2931; 2837	1685; 1449; 1363; 1192; 1157; 1085; 1035; 1019	964; 916; 857; 762; 712
ARP/DIMEB + MCE	3402; 2921	1686; 1450; 1365; 1191; 1155; 1085; 1043; 1017	963; 917; 857; 762; 710

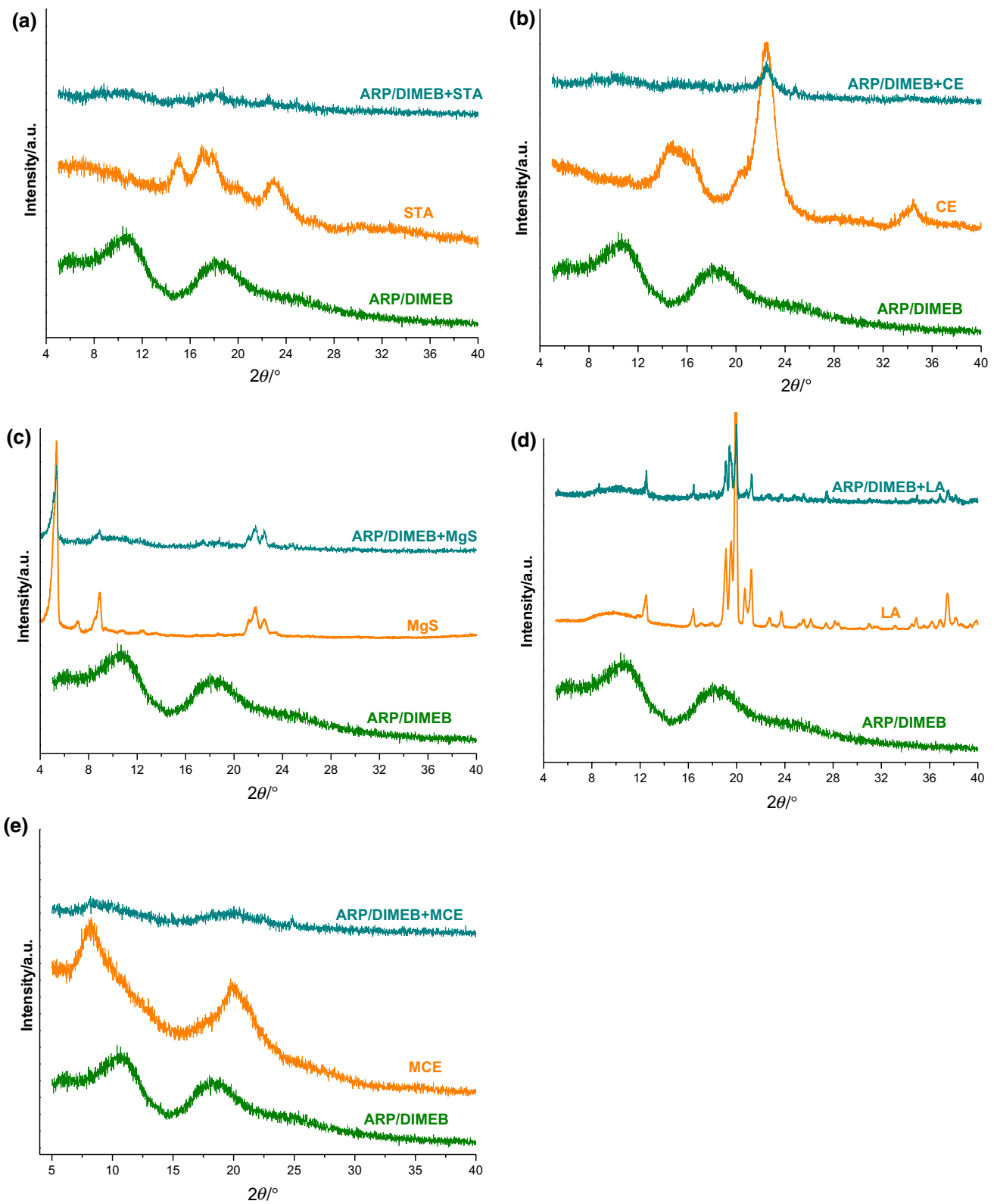


Fig. 10 Powder X-ray diffractogram profiles of ARP/DIMEB and every selected excipient: **a** STA; **b** CE; **c** MgS; **d** LA and **e** MCE

last case, an interaction between ARP/DIMEB and MgS is revealed, since several bands of the complex (namely the ones appearing at 3404, 1155 and 917 cm^{-1} , respectively) are no longer present in the spectra of mixture with this excipient. Interactions are not suggested for other mixtures under ambient temperature by this technique, leading to the conclusion that the incompatibility with MCE is thermally induced.

PXRD analysis

In order to assess the potential interactions between ARP/DIMEB inclusion complex and excipients, which correlate with changes in the crystallinity of the samples, X-ray diffractometry was used as a complementary tool. The PXRD patterns of the ARP/DIMEB complex and its physical mixture with previously mentioned excipients recorded in identical conditions are shown in Fig. 10.

The diffractogram of ARP/DIMEB inclusion complex reveals two main broad peaks and numerous undefined ones, with low intensities clearly indicating an amorphous state. According to the obtained data, amorphization is even further advanced after trituration of complex with excipient, as in the case of mixtures with STA, CE and MCE (Fig. 10a, b, e). The PXRD profile of MgS reveals characteristic diffraction peaks at 2θ of 5.35, 7.20, 8.90, 21.78 and 22.53 indicating the crystalline nature of the excipient (Fig. 10c). Also, the crystalline profile of LA is proven by the sharp and intense peaks at 12.46, 16.42, 19.12, 19.51, 19.94, 20.72 and 21.19 2θ which are present in its diffraction pattern (Fig. 10d).

The PXRD pattern of physical mixture of inclusion complex with MgS contains most the characteristic excipient peaks (at 5.34; 21.78 and 22.45 2θ values); while the peak at 8.92 2θ is highly alliterated and the one from 7.20 is no longer visible. Even if it plausible to explain that the alliteration/disappearance of peaks that appear for pure excipient below 10.00 2θ values is due to dilution effect, an in-depth analysis reveals that the disappearance is due to solid-state interaction that takes place between the complex and MS—confirmed by the fact that the peaks of excipient from 21.78 to 22.45 2θ values are still present, unadulterated in comparison with pure excipient. Following this observation, the interaction suggested by thermal analysis and FTIR spectroscopy is also confirmed by this instrumental technique.

In the case of mixture with LA (peaks at 12.53, 16.45, 19.01, 19.39, 19.99, 20.83 and 21.23, respectively 2θ values), the bands of excipient are entirely visible in the diffraction pattern, as in the case of pure excipient—but with a corresponding decrease of intensity due to dilution effect. The PXRD data suggest compatibility between complex and LA, incompatibility between complex and MgS, while

the information for the mixtures with STA, CE and MCE is inconclusive by themselves, revealing solely the advanced amorphization of samples during mixing.

Conclusions

In this current work, a supramolecular adduct represented by an inclusion complex of poorly water-soluble drug ARP with a methylated β -cyclodextrin, namely DIMEB, was obtained and characterized by theoretical and experimental approaches. Our results achieved by applying Job's method indicate a stoichiometry of 1:2 for ARP/DIMEB inclusion complex. The thermal and spectroscopic techniques used for the evaluation of inclusion complex in solid state demonstrate different physicochemical properties of the kneaded product in comparison with pure precursors, thus proving the obtaining of real inclusion complex when the kneading method is employed. The ARP solubility is increased by 37.87-fold in the presence of DIMEB, which demonstrates the utility of the cyclodextrin in improving ARP physicochemical properties and consecutively its biopharmaceutical profile.

Also, the compatibility of the ARP/DIMEB inclusion complex with five excipients used in the pharmaceutical formulation, namely starch, microcrystalline cellulose, magnesium stearate, lactose monohydrate and methylcellulose, is also evaluated by means of thermoanalytical and spectroscopic methods. FTIR analysis suggested chemical interactions solely between ARP/DIMEB inclusion complex and MgS, while with all other excipients showed compatibility. The incompatibility in the system ARP/DIMEB + MgS is also confirmed by the PXRD study, this second investigational technique revealing also the advanced amorphization of components during mixing of complex with STA, CE and MCE.

Thermoanalytical data suggested that thermally induced interactions take place between the components in the systems containing MgS and MCE, while STA, CE and LA can be safely used as excipients in developing solid formulations containing ARP/DIMEB inclusion complex as active pharmaceutical ingredient. The results of this study reinforce the applicability of thermal methods along with FTIR and PXRD as fast, precise and reproducible screening tools for analysis of API–excipient compatibility in the preformulation stage of drug development.

References

1. Magliocco F, de Filippis R, Aloi M, Staltari FA, Gaetano R, Segura-Garcia C, De Fazio P. Second-generation long-acting injections anti-psychotics improve executive functions in patients with schizophrenia: a 12-month real-world study. *Int J Psychiatry Clin Pract.* 2020. <https://doi.org/10.1080/13651501.2020.1737134>.

2. Azorin JM, Simon N. Dopamine receptor partial agonists for the treatment of bipolar disorder. *Drugs*. 2019;79(15):1657–77.
3. Simon N, Azorin JM. Aripiprazole as dopamine partial agonist model: basic concepts and clinical impact. *Encephale*. 2018;44(6):558–64.
4. Saxena K, Kurian S, Saxena J, Goldberg A, Chen E, Simonetti A. Mixed states in early-onset bipolar disorder. *Psychiatr Clin North Am*. 2020;43(1):95–111.
5. Censi R, Di Martino P. Polymorph impact on the bioavailability and stability of poorly soluble drugs. *Molecules*. 2015;20(10):18759–76.
6. Wu Y, Cheng L, Wu J, Zhai M, Cai L. Cosolvent effect on solubility of aripiprazole in mixed solvents and apparent thermodynamic analysis of dissolution process. *J Chem Thermodyn*. 2019;135:330–5.
7. Ardiana F, Lestari MLAD, Indrayanto G. Chapter two—aripiprazole. In: Brittain HG (ed) *Profiles drug subst. excip. relat. methodol.* Academic Press, pp 35–85.
8. Brittain HG. Aripiprazole: polymorphs and solvatomorphs. *Profiles Drug Subst Excip Relat Methodol*. 2012;37:1–29.
9. Tan X, Zhong Y, He L, Zhang Y, Jing G, Li S, Wang J, He H, Tang X. Morphological and crystalline transitions in monohydrated and anhydrous aripiprazole for a long-acting injectable suspension. *AAPS Pharm Sci Tech*. 2017;18(4):1270–6.
10. Zeidan TA, Trotta JT, Chiarella RA, Oliveira MA, Hickey MB, Almarsson Ö, Remenar JF. Polymorphism of dehydro-aripiprazole, the active metabolite of the antipsychotic drug aripiprazole (abilify). *Cryst Growth Des*. 2013;13(5):2036–46.
11. Braun DE, Gelbrich T, Kahlenberg V, Tessadri R, Wieser J, Griesser UJ. Stability of solvates and packing systematics of nine crystal forms of the antipsychotic drug aripiprazole. *Cryst Growth Des*. 2009;9(2):1054–65.
12. Łyszczarz E, Hofmanová J, Szafraniec-Szczyński J, Jachowicz R. Orodispersible films containing ball milled aripiprazole-poloxamer®407 solid dispersions. *Int J Pharm*. 2020. <https://doi.org/10.1016/j.ijpharm.2019.118955>.
13. Ramya AR, Sudheer P, Mohameed AS, Das AK. Design and evaluation of a self-emulsifying drug delivery system of aripiprazole. *Indian J Pharm Sci*. 2019;81(6):1089–98.
14. McFall H, Sarabu S, Shankar V, Bandari S, Murthy SN, Kolter K, Langley N, Kim DW, Repka MA. Formulation of aripiprazole-loaded pH-modulated solid dispersions via hot-melt extrusion technology: in vitro and in vivo studies. *Int J Pharm*. 2019;554:302–11.
15. Nanubolu JB, Ravikumar K. Correlating the melting point alteration with the supramolecular structure in aripiprazole drug cocrystals. *Cryst Eng Comm*. 2016;18(6):1024–38.
16. Abdelbary AA, Li X, El-Nabarawi M, Ellassasy A, Jasti B. Comparison of nanomilling and coprecipitation on the enhancement of in vitro dissolution rate of poorly water-soluble model drug aripiprazole. *Pharm Dev Technol*. 2014;19(4):491–500.
17. Fernández Casares A, Nap WM, Ten Figás G, Huizenga P, Groot R, Hoffmann M. An evaluation of salt screening methodologies. *J Pharm Pharmacol*. 2015;67(6):812–22.
18. Oh YJ, Choi G, Choy Bin Y, Park JW, Park JH, Lee HJ, Yoon YJ, Chang HC, Choy JH. Aripiprazole-montmorillonite: a new organic–inorganic nanohybrid material for biomedical applications. *Chem Eur J*. 2013;19(15):4869–75.
19. Mihajlovic T, Kachrimanis K, Graovac A, Djuric Z, Ibric S. Improvement of aripiprazole solubility by complexation with (2-hydroxy)propyl-β-cyclodextrin using spray drying technique. *AAPS Pharm Sci Tech*. 2012;13(2):623–31.
20. Badr-Eldin SM, Ahmed TA, Ismail HR. Aripiprazole-cyclodextrin binary systems for dissolution enhancement: effect of preparation technique, cyclodextrin type and molar ratio. *Iran J Basic Med Sci*. 2013;16(12):1223–31.
21. Tănase IM, Sbârcea L, Ledeti A, Vlase G, Barvinschi P, Văruț RM, Dragomirescu A, Axente C, Ledeti I. Physicochemical characterization and molecular modeling study of host–guest systems of aripiprazole and functionalized cyclodextrins. *J Therm Anal Calorim*. 2020. <https://doi.org/10.1007/s10973-020-09549-3>.
22. Trandafirescu C, Ledeti I, Șoica C, Ledeti A, Vlase G, Borcan F, Dehelean C, Coricovac D, Racoviceanu R, Aigner Z. Albendazole-cyclodextrins binary systems: thermal and spectral investigation on drug-excipient interaction. *J Therm Anal Calorim*. 2019;138(5):3039–54.
23. Circioban D, Ledeti A, Vlase G, Moaca A, Ledeti I, Farcas C, Vlase T, Dehelean C. Thermal degradation, kinetic analysis and evaluation of biological activity on human melanoma for artemisinin. *J Therm Anal Calorim*. 2018;134(1):741–8.
24. Kim DH, Lee SE, Pyo YC, Tran P, Park JS. Solubility enhancement and application of cyclodextrins in local drug delivery. *J Pharm Investig*. 2020;50(1):17–27.
25. D’Aria F, Serri C, Niccoli M, Mayol L, Quagliariello V, Iaffaioli RV, Biondi M, Giancola C. Host–guest inclusion complex of quercetin and hydroxypropyl-β-cyclodextrin: a calorimetric study. *J Therm Anal Calorim*. 2017;130(1):451–6.
26. de Lima Ramos Júnior FJ, da Silva KMA, Brandão DO, et al. Investigation of the thermal behavior of inclusion complexes with antifungal activity. *J Therm Anal Calorim*. 2018;133(1):641–8.
27. Ohata T, Ikeda H, Mizobe T, Yukawa M, Aki H. Effect of solution pH on complex formation between epi-type catechin and β-cyclodextrin. *J Therm Anal Calorim*. 2019;135(5):2837–41.
28. Ikeda H, Ohata T, Yukawa M, Fujisawa M, Aki H. Difference in formation mechanism of inclusion complex between configuration isomers of gallate-type catechin and β-cyclodextrin. *J Therm Anal Calorim*. 2019;135(5):2789–95.
29. Pires FQ, Pinho LA, Freire DO, Silva ICR, Sa-Barreto LL, Cardozo-Filho L, Gratieri T, Gelfuso GM, Cunha-Filho M. Thermal analysis used to guide the production of thymol and Lippia origanoides essential oil inclusion complexes with cyclodextrin. *J Therm Anal Calorim*. 2019;137(2):543–53.
30. Usacheva T, Kabirov D, Beregova D, Gamov G, Sharnin V, Biondi M, Mayol L, D’Aria F, Giancola C. Thermodynamics of complex formation between hydroxypropyl-β-cyclodextrin and quercetin in water–ethanol solvents at T = 298.15 K. *J Therm Anal Calorim*. 2019;138(1):417–24.
31. Sbârcea L, Ledeti A, Udrescu L, Văruț RM, Barvinschi P, Vlase G, Ledeti I. Betulonic acid–cyclodextrins inclusion complexes. *J Therm Anal Calorim*. 2019;138(4):2787–97.
32. Oliva R, Battista F, Cozzolino S, Notomista E, Winter R, Del Vecchio P, Petraccone L. Encapsulating properties of sulfobutylether-β-cyclodextrin toward a thrombin-derived antimicrobial peptide. *J Therm Anal Calorim*. 2019;138(5):3249–56.
33. Abilify. <https://www.drugs.com/pro/abilify.html>. Accessed 13 April 2020.
34. Zhang L, Luan H, Lu W, Wang H. Preformulation studies and enabling formulation selection for an insoluble compound at pre-clinical stage—from in vitro, in silico to in vivo. *J Pharm Sci*. 2020;109(2):950–8.
35. Noonan TJ, Chibale K, Bourne SA, Caira MR. A preformulation co-crystal screening case study: polymorphic co-crystals of an imidazopyridazine antimalarial drug lead with the conformer succinic acid. *J Mol Struct*. 2020. <https://doi.org/10.1016/j.molstruc.2019.127561>.
36. Rathod VR, Shah DA, Dave RH. Systematic implementation of quality-by-design (QbD) to develop NSAID-loaded nanostructured lipid carriers for ocular application: preformulation screening studies and statistical hybrid-design for optimization of variables. *Drug Dev Ind Pharm*. 2020;46(3):443–55.
37. Kacso I, Rus LM, Martin F, Miclaus M, Filip X, Dan M. Solid-state compatibility studies of ketoconazole-fumaric acid co-crystal

- with tablet excipients. *J Therm Anal Calorim.* 2020. <https://doi.org/10.1007/s10973-020-09340-4>.
38. Arnfast L, van Renterghem J, Aho J, Bøtker J, Raijada D, Baldursdóttir S, De Beer T, Rantanen J. Exploring the complexity of processing-induced dehydration during hot melt extrusion using in-line Raman spectroscopy. *Pharmaceutics.* 2020. <https://doi.org/10.3390/pharmaceutics12020116>.
 39. Ledeti I, Romanescu M, Cîrcioban D, et al. Stability and compatibility studies of levothyroxine sodium in solid binary systems—instrumental screening. *Pharmaceutics.* 2020;12(1):58.
 40. Sbârcea L, Ledeti I, Drăgan L, Kurunczi L, Fuliaş A, Udrescu L. Fosinopril sodium-hydroxypropyl- β -cyclodextrin inclusion complex: thermal decomposition kinetics and compatibility studies. *J Therm Anal Calorim.* 2015;120(1):981–90.
 41. Udrescu L, Sbârcea L, Fuliaş A, Ledeti I, Vlase G, Barvinschi P, Kurunczi L. Physicochemical analysis and molecular modeling of the Fosinopril β -cyclodextrin inclusion complex. *J Spectrosc.* 2014. <https://doi.org/10.1155/2014/748468>.
 42. Benesi HA, Hildebrand JH. A Spectrophotometric Investigation of the interaction of iodine with aromatic hydrocarbons. *J Am Chem Soc.* 1949;71(8):2703–7.
 43. Srinivasan K, Stalin T, Sivakumar K. Spectral and electrochemical study of host-guest inclusion complex between 2,4-dinitrophenol and β -cyclodextrin. *Spectrochim Acta Part A Mol Biomol Spectrosc.* 2012;94:89–100.
 44. Protein Data Bank. <http://www.pdb.org/pdb/home/home.do>. Accessed 15 November 2019.
 45. DeLano WL. PyMOL, San Carlos, CA, 700, 2002.
 46. Job P. Formation and stability of inorganic complexes in solution. *Ann di Chim Appl.* 1928;9:113–203.
 47. Sbârcea L, Udrescu L, Ledeti I, Szabadai Z, Fuliaş A, Sbârcea C. β -Cyclodextrin inclusion complexes of lisinopril and zofenopril: physicochemical characterization and compatibility study of lisinopril- β -cyclodextrin with lactose. *J Therm Anal Calorim.* 2016;123(3):2377–90.
 48. Sbârcea L, Udrescu L, Drăgan L, Trandafirescu C, Szabadai Z, Bojiţă M. Fosinopril-cyclodextrin inclusion complexes: phase solubility and physicochemical analysis. *Pharmazie.* 2011;66(8):584–9.
 49. Doile MM, Fortunato KA, Schmücker IC, Schucko SK, Silva MAS, Rodrigues PO. Physicochemical properties and dissolution studies of dexamethasone acetate- β -cyclodextrin inclusion complexes produced by different methods. *AAPS Pharm Sci Tech.* 2008;9(1):314–21.
 50. Cîrcioban D, Ledeti A, Vlase G, Coricovac D, Moaca A, Farcas C, Vlase T, Ledeti I, Dehelean C. Guest–host interactions and complex formation for artemisinin with cyclodextrins: instrumental analysis and evaluation of biological activity. *J Therm Anal Calorim.* 2018;134(2):1375–84.
 51. Mennini N, Maestrelli F, Cirri M, Mura P. Analysis of physicochemical properties of ternary systems of oxaprozin with randomly methylated- β -cyclodextrin and L-arginine aimed to improve the drug solubility. *J Pharm Biomed Anal.* 2016;129:350–8.
 52. Huey R, Morris GM, Olson AJ, Goodsell DS. A semiempirical free energy force field with charge-based desolvation. *J Comput Chem.* 2007;28(6):1145–52.
 53. Baka E, Comer JEA, Takács-Novák K. Study of equilibrium solubility measurement by saturation shake-flask method using hydrochlorothiazide as model compound. *J Pharm Biomed Anal.* 2008;46(2):335–41.
 54. Udrescu L, Sbârcea L, Fuliaş A, Ledeti I, Vlase T, Barvinschi P, Kurunczi L. Physicochemical characterization of zofenopril inclusion complex with 2-hydroxypropyl- β -cyclodextrin. *J Serbian Chem Soc.* 2015;80(4):485–97.
 55. Udrescu L, Fuliaş A, Ledeti I, Vlase G, Barvinschi P, Kurunczi L, Sbârcea L. Host-guest system of zofenopril and randomly methylated β -cyclodextrin. *Rev Chim.* 2015;66(1):17–20.
 56. Rus LM, Iurian S, Kacso I, Borodi G, Porav S, Hegheş SC, Iuga CA, Tomuţa I. Development of meloxicam oral lyophilisates: role of thermal analysis and complementary techniques. *Farmacia.* 2019;67(1):56–67.
 57. Cristea M, Baul B, Ledeti I, et al. Preformulation studies for atorvastatin calcium: an instrumental approach. *J Therm Anal Calorim.* 2019;138(4):2799–806.

Publisher's Note Springer Nature remains neutral with regard to jurisdictional claims in published maps and institutional affiliations.